Journal of The Electrochemical Society, **164** (14) E529-E535 (2017)
0013-4651/2017/164(14)/E529/7/$37.00 © The Electrochemical Society

Mass-Transfer Study and Copper Ions Removal Using a Modified Hydrocyclone as Electrochemical Reactor

L. C. Resio, O. González Pérez, and J. M. Bisang[z]

Universidad Nacional del Litoral, CONICET, Programa de Electroquímica Aplicada e Ingeniería Electroquímica (PRELINE), Facultad de Ingeniería Química, S3000AOM Santa Fe, Argentina

Mass-transfer coefficients between an electrolyte solution and the wall of a hydrocyclone were experimentally determined by using the electrochemical technique. The local mass-transfer coefficients were measured as a function of the axial distance from the entrance changing the inlet volumetric flow rate and the underflow stream. An enhancement of mass-transfer was observed in comparison to that predicted for developing axial flow in an annular duct, being the cylindrical part more active than the conical one. The global mass-transfer coefficient in the cylindrical region depends on the Reynolds number raised to an exponent of 0.79, in accordance with the mass-transfer behavior of decaying annular swirl flow. The modified hydrocyclone was also examined for the removal of copper from dilute synthetic solutions. A diminution of copper concentration from 400 ppm to 40 ppm was achieved after 60 minutes of electrolysis in a recirculating system and the contaminant was recovered as a metal powder separated by the hydrocyclone. The space time yield and the specific energy consumption were 12.5 kg m^{-3} h^{-1} and 4.9 kW h kg^{-1}, respectively, with a cumulative current efficiency of 54%, showing that the modified hydrocyclone is a suitable reactor for the electrochemical treatment of effluents.

Manuscript received September 26, 2017. Published December 6, 2017.

Hydrocyclones are used in chemical engineering for the centrifugal separation of materials contained in the feed liquid. These materials may be particles of solid, bubbles of gas or a second immiscible liquid. In the case of two solids suspended in the feed liquid they may separate because of a difference in size, shape, or specific gravity.[1,2] Another application domain of hydrocyclones is in electrochemical engineering, and particularly for the improvement of electrochemical removal of contaminants from dilute solutions. This device is recognized for its inherent simplicity, without moving parts, and modular design making it attractive for industrial applications. Thus, Dhamo et al.[3,4] and Dhamo[5] studied the removal of copper and silver in a hydrocyclone cell using the stainless steel wall as a cathode and the anode, made of graphite or stainless steel, was placed in the top opening surrounded by a cationic exchange membrane which acts as a vortex finder. The global mass-transfer coefficients are also reported. The same device was employed for the simultaneous oxidation of cyanide at a graphite anode during the electrodeposition of silver.[6] Rajalo and coworkers[7] applied a hydrocyclone cell for the electrochemical oxidation of sulfide and thiosulfate from tannery waste waters. The vortex finder made of titanium coated with manganese dioxide worked as an anode and the stainless steel wall of the hydrocyclone as a cathode. Sundmacher[8] proposed an electrochemical cell based on a double cyclone to obtain well-defined mass-transfer conditions for the characterization of gas-diffusion electrodes. Kim et al. analyzed the performance of a modified cyclone cell for the electrowinning of palladium[9] and platinum.[10] A titanium cylinder was used as a cathode placed in the cylindrical part of the hydrocyclone and a graphite tube worked simultaneously as anode and vortex finder. Rhodium electrowinning was carried out in a similar equipment using a stainless steel tube as anode.[11] High values of the global mass-transfer coefficients are reported in terms of a dimensionless correlation.

The aim of the present contribution was to analyze the variation of the local mass-transfer coefficient at the wall of the hydrocyclone as a function of the axial position from the entrance in order to identify the more active regions of the equipment. A second goal was to carry out the removal of a metal from a dilute synthetic effluent and the recovery of the product as a metal powder. Thus, the modified hydrocyclone allows the treatment of a wastewater simultaneously with the transformation of the contaminant and its separation into a product of commercial value.

Experimental

Mass-transfer studies.—All experiments were performed in an electrochemical reactor based in a modified hydrocyclone, as is shown schematically in Fig. 1. The reactor was made of two parallelepiped blocks of acrylic material, 80 mm side and 108 mm length for the upper block and 125 mm length for the lower block. The cylindrical part of the hydrocyclone was machined in the upper block and the conical part in the lower one. Both blocks were assembled by a threaded joint.

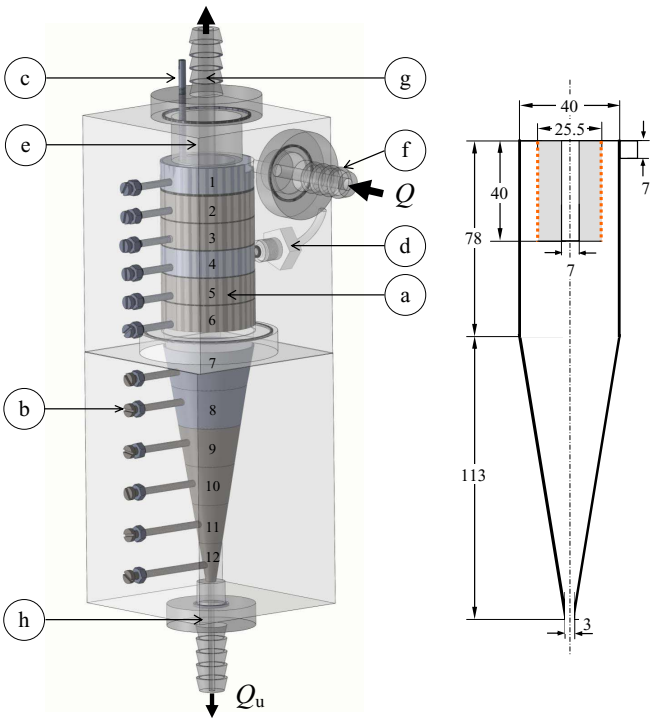

Figure 1. Schematic representation of the modified electrochemical hydrocyclone reactor. (a) Segmented cathode; (b) electrical connections to calibrated resistors; (c) electrical connection to anode; (d) Luggin capillary for cathodic potential control; (e) vortex finder; (f) electrolyte inlet; (g) electrolyte overflow; (h) spigot. The numbers indicate the position of the segments and the arrows the flow of the electrolyte. Q: inlet volumetric flow rate. Q_u: underflow stream. Right hand side: thick full line: cathode; thick dotted line: anode. Internal dimensions of the hydrocyclone in mm.

[z]E-mail: jbisang@fiq.unl.edu.ar

Table I. Physicochemical properties of the ferricyanide/ferrocyanide solution.

Composition	$[K_3Fe(CN)_6] = 5 \times 10^{-2}$ mol dm^{-3} $[K_4Fe(CN)_6] = 0.1$ mol dm^{-3} $[K_2CO_3] = 1.75$ mol dm^{-3}
ν / m^2 s^{-1}	1.52×10^{-6}
D / m^2 s^{-1}	5×10^{-10}
Sc	3040

In the internal wall of the hydrocyclone was arranged the segmented cathode which was made of 12 segments of 316 stainless steel, six in the cylindrical part and six in the conical part. The cylindrical segments were 40 mm internal diameter and 12 mm length and the conical segments 18 mm length. The segments were insulated from one another by a polyamide ring 1 mm thick. Thus, the total length of the cylindrical body was 78 mm and the length with segments in the conical part was 113 mm with an angle of 18°. The anode was made of a 316 stainless steel tube, 25.5 mm external diameter and 40 mm length. The vortex finder, 7 mm diameter, was concentric with the anode. The bottom opening was 3 mm diameter. The scheme on the right hand side of Fig. 1 summarizes the internal dimensions of the hydrocyclone which correspond to those of a standardized equipment.[1] The surface of the working electrode was polished with emery paper 2500 and it was washed with distilled water. Calibrated resistors, 0.025 Ω resistance, were inserted between the back side of each segment and the cathodic current feeder, which was electrically connected at both ends. By measuring the ohmic drop in the resistors, it was possible to determine the axial current distribution and to calculate the local mass-transfer coefficient at each segment. The effect of the calibrated resistors on the current distribution can be neglected due to the small value of their ohmic drop, approximately 10 mV, in comparison with the other terms of the voltage balance in the reactor. The data acquisition was performed using a computer controlled home made analogue multiplexer. During an experiment all the segments were connected to the cathodic current feeder. The experiments were carried out potentiostatically at potentials ranging from −0.7 V to −0.85 V, verifying that a limiting current was achieved. The cathodic potential was controlled against a saturated calomel electrode, SCE, connected to a Haber-Luggin capillary positioned in the cylindrical body at 45 mm from the top. The interelectrode gap in the cylindrical part was 7.25 mm and the electrolyte volume inside hydrocyclone was 0.1526 dm^3. The volume of solution in each run amounted to capacity 5 dm^3.

The reactor was made part of a flow circuit system consisting of a pump, a flowmeter, a reservoir and connections to maintain the temperature at the preset value, 30°C. The inlet volumetric flow rate, Q, was changed in the range of 6 to 10 dm^3 min^{-1} and the underflow stream, Q_u, was varied between 0 and 1.7 dm^3 min^{-1}.

The test reaction for the mass-transfer studies was the electrochemical reduction of ferricyanide with $[K_3Fe(CN)_6] \cong 0.05$ mol dm^{-3} or lower and $[K_4Fe(CN)_6] \cong 0.1$ mol dm^{-3} in 1.75 mol dm^{-3} of K_2CO_3 as supporting electrolyte, while the reverse reaction occurred at the anode. Nitrogen was bubbled in the reservoir for 1 h prior to the experiment with the aim of remove the dissolved oxygen. A large difference in concentration between ferricyanide and ferrocyanide was chosen in order to avoid a secondary reaction at the stainless steel anode due to its smaller surface area. The high concentration of supporting electrolyte was adopted to diminish the oxygen solubility in the electrolyte.[12] Thus, the current for the reduction of the residual oxygen after bubbling nitrogen is negligible in comparison with the reduction current of ferricyanide from this dilute solution. Table I summarizes the composition and physicochemical properties of the electrolyte. Samples of the solution were taken from the reservoir after each experiment and the ferricyanide concentration was spectrophotometrically determined using 10 mm quartz absorption cells and the supporting electrolyte was used as blank. The measurements were performed at a wavelength of 420 nm, where it is possible to determine the ferricyanide concentration without any interference of ferrocyanide.

The local mass-transfer coefficient, $k_{m,y}$, was calculated from the limiting current at each segment, $I_{lim,i}$, and the reactant bulk concentration, c, using the following equation.[13]

$$k_{m,y} = \frac{I_{lim,i}}{\nu_e F A_i c} \quad [1]$$

Removal of copper.—The same modified hydrocyclone was also used in the experiment of copper removal from dilute solutions. In this case, to avoid the corrosion, the anode was electroplated with lead using a fluoborate bath[14] to get a lead thickness of 50 μm. The electrolyte solution was 1 M Na_2SO_4 and H_2SO_4, to obtain pH 2, with a copper concentration of approximately 400 ppm, unless otherwise is stated. Thus, the reduction of copper ions occurs at the cathode, according to:

$$Cu^{2+} + 2e^- \rightarrow Cu \quad [2]$$

Likewise, oxygen evolution takes place at the anode:

$$H_2O \rightarrow \frac{1}{2}O_2 + 2H^+ + 2e^- \quad [3]$$

The inverse of reaction [3] can occur also at the cathode lowering the current efficiency for copper deposition. During an experiment samples of the solution were taken from the reservoir from time to time and the copper concentration, c, was spectrophotometrically determined according to the method described by Mehlig[15] at a wavelength of 624 nm and using the supporting electrolyte as blank. The experiments were performed under potentiostatic control, frequently at −0.65 V against SCE, where copper deposition takes place without hydrogen evolution as secondary reaction.[16] Both, cell potential difference, U, and current, I, were measured as a function of time.

From the above measurements, the values of the cumulative current efficiency, β, the specific energy consumption, E_s, the space time yield, ρ, and the normalized space velocity, s_n, were calculated with the following equations:

$$\beta(t) = \frac{\nu_e F V\,[c(0) - c(t)]}{M \int_0^t I(t)\mathrm{d}t} \quad [4]$$

$$E_s(t) = \frac{\int_0^t I(t)U(t)\mathrm{d}t}{V\,[c(0) - c(t)]} \quad [5]$$

$$\rho = \frac{V\,[c(0) - c(t)]}{V_r t} \quad [6]$$

and

$$s_n = -\frac{\ln\left[\frac{c(t)}{c(0)}\right]}{t \ln 10} \quad [7]$$

Results and Discussion

Mass-transfer studies.—Fig. 2 reports on a typical result of the local mass-transfer coefficient as a function of the axial position in the reactor for different values of the applied potential at the cathode. The segments are numbered from top (1) to bottom (12), as shown in Fig. 1. The symbols at each potential correspond to the average value of ten independent measurements. Likewise, the close agreement between the data at different potentials, in the range from −0.7 V to −0.85 V, demonstrates that limiting current conditions were achieved at each segment. A similar kinetic behavior was previously reported using a rotating disc electrode,[17] where it was stated that the reduction of ferricyanide from a solution of K_2CO_3 as supporting electrolyte at a 316 stainless steel cathode shows a mass-transfer control in a wide

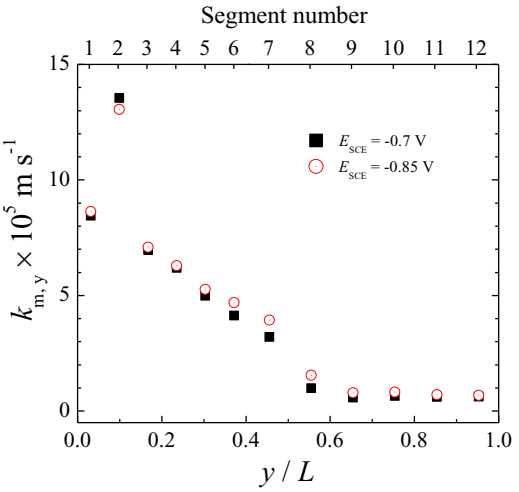

Figure 2. Local mass-transfer coefficient as a function of the axial position for different values of applied potential at the cathode. $Q = 6$ dm^3 min^{-1}, $Q_u = 0.87$ dm^3 min^{-1}. Ferricyanide reduction as test reaction.

range of potentials for values more negative than −0.6 V, beginning hydrogen evolution at −1.2 V. Thus, the present results confirm the previous data.

Fig. 3 reports on typical curves of the local mass-transfer coefficient as a function of the axial position in the reactor for different values of both inlet volumetric flow rate, Q, and underflow stream, Q_u. The symbols correspond to the results of ten independent measurements. The thin full line joins the average values of the local mass-transfer coefficient at each segment and the error bars represent the standard deviation. A good reproducibility of the results is detected. In part (a), only the second segment in the cylindrical body presents a high scattering of the experimental data, which can be attributable to the influence of the electrolyte inlet, where a direct jetting effect takes place, and also to the eddy and short circuit flows in this region.[1] The local mass-transfer coefficients show a peak in the second segment and a monotonous decrease with the axial position in the hydrocyclone. The same behavior with a peak near the entrance region was also reported in mass-transfer studies under decaying annular swirl flow.[18] Moreover, in the cylindrical body the values are higher than those in the conical part, despite the accelerated downward helical flow along this region with a flow pattern formed by an inner spiral within an outer spiral rotating in the same direction.[1] The low values of the mass-transfer coefficient in the conical part can be explained taking into account that at the entrance region both the diffusion boundary layer and the hydrodynamic boundary layer develop from the same point. When the diffusion boundary layer is developing the mass-transfer rate decreases approaching a constant value downstream when the diffusion boundary layer is established. Similarly, as the hydrodynamic boundary layer develops the mass-transfer rate also decrease. Then, lower local mass-transfer coefficients are expected along the axial length when both boundary layers are developing. The thick full line represents the global mass-transfer coefficient, $k_{m,\,global}$, calculated in accordance to:

$$k_{m,global} = \frac{\sum_{i=1}^{12} k_{m,y} A_i}{\sum_{i=1}^{12} A_i} \quad [8]$$

The mass transfer coefficient in a smooth annular duct with axial developing flow is given by:[19]

$$Sh = 1.029 Re^{0.55} Sc^{1/3} \left(\frac{L}{d_e}\right)^{-0.472} \quad [9]$$

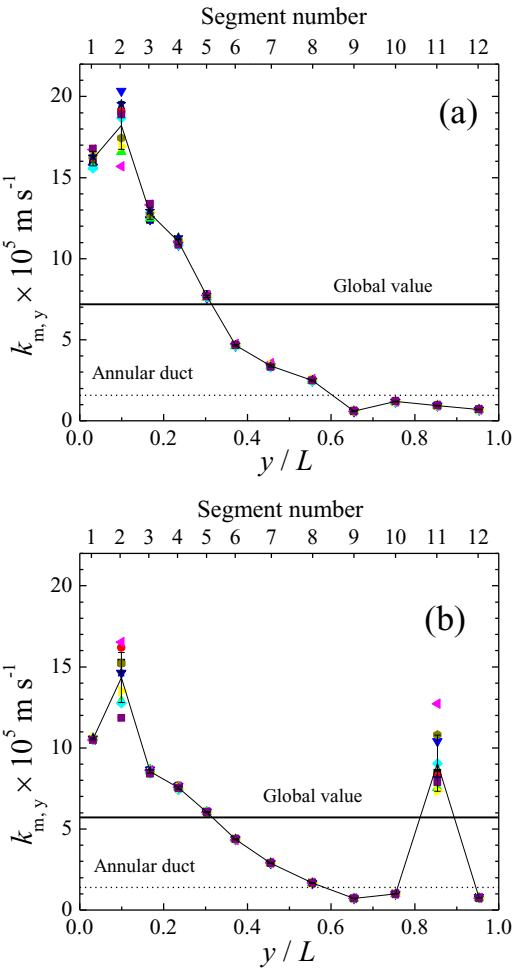

Figure 3. Local mass-transfer coefficient as a function of the axial position. Part (a): $Q = 10$ dm^3 min^{-1}, $Q_u = 1.67$ dm^3 min^{-1}. Part (b): $Q = 8$ dm^3 min^{-1}, $Q_u = 0.87$ dm^3 min^{-1}. $E_{SCE} = -0.85$ V. Ten independent measurements. Thin full line: average value of the local mass-transfer coefficient at each segment. Error bars: standard deviation. Thick full line: global mass-transfer coefficient. Dashed line: global mass-transfer coefficient for an annular duct with axial flow according to Eq. 9. Ferricyanide reduction as test reaction.

being Sh, Re and Sc the Sherwood, Reynolds and Schmidt numbers, respectively. Eq. 9 is valid for $400 < Re < 2000$, $1100 < Sc < 5200$ and $6.8 < L / d_e < 34.4$. In order to have a basis for evaluating the degree of mass-transfer enhancement, the mass-transfer coefficient according to Eq. 9 is represented as a dashed line in Fig. 3. It can be seen that the global mass-transfer coefficient for the modified hydrocyclone is higher than that for an annular duct with developing axial flow, revealing the good performance of the equipment. However, this beneficial aspect is counteracted by the high pressure drop of the hydrocyclone. Fig. 3, part (b) displays the distribution of the local mass transfer coefficient for a different combination of flow rates. The conclusions from part (b) are similar to those of part (a) with only a difference given by that the penultimate segment in the conical part shows a high value of the local mass-transfer coefficient with an important scattering of the results between the different measurements, probably due to the eddies formation near to the spigot under these hydrodynamic conditions. This abnormal situation in the penultimate segment in the conical part takes place in the middle range of examined underflow streams. At low and high underflows a monotonous decrease in the local mass-transfer coefficient in the conical part was measured, as it is reported on part (a).

Fig. 4 shows the dimensionless ratio between local and global mass-transfer coefficients as a function of the axial position in the

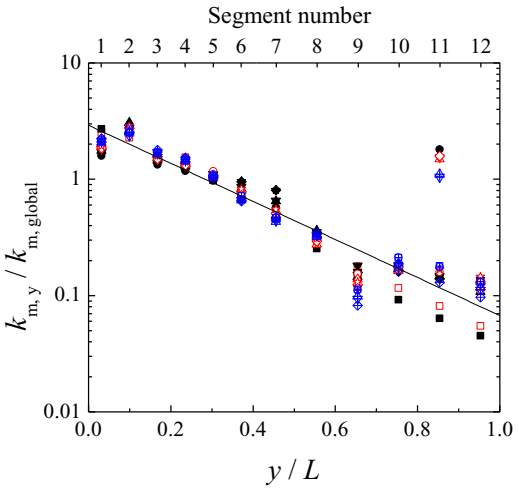

Figure 4. Dimensionless ratio between the local and global mass-transfer coefficients as a function of the axial position. Full symbols: $Q = 6$ dm^3 min^{-1}. Open symbols: $Q = 8$ dm^3 min^{-1}. Centered symbols: $Q = 10$ dm^3 min^{-1}. Ferricyanide reduction as test reaction.

hydrocyclone for different underflows and inlet volumetric flow rates. Neglecting the abnormal experimental data for the penultimate segment in the conical part, the experimental results are correlated by the following empirical relationship, represented as full line in Fig. 4:

$$\frac{k_{m,y}}{k_{m,global}} = 2.912 \exp\left(-3.77 \frac{y}{L}\right) \quad [10]$$

The influence of the underflow stream on the global mass-transfer coefficient for different values in the inlet volumetric flow rate is analyzed in Fig. 5. The dashed line represents the mean values showing that the underflow has no effect on the mass-transfer in the hydrocyclone.

Fig. 6 compares, in double logarithmic coordinates, the global mass-transfer coefficients as a function of the inlet volumetric flow rate for the hydrocyclone, full line, with those for the cylindrical part, CP, of this reactor, dashed line. The correlation equations are also reported on the figure and Eq. 11 gives the dimensionless relationship for the mass-transfer in the cylindrical part of the hydrocyclone.

$$Sh_{CP} = 0.513 Re^{0.79} Sc^{1/3} \quad [11]$$

The exponent of the volumetric flow rate in Eq. 11 is similar to those suggested by Dhamo.[5] Likewise, an exponent near 0.8 is in close

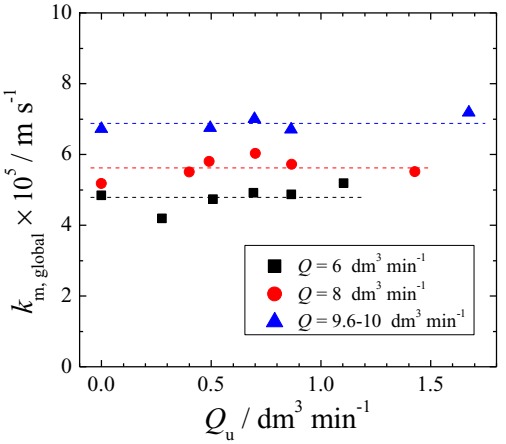

Figure 5. Influence of the underflow stream on the global mass-transfer coefficient. Ferricyanide reduction as test reaction.

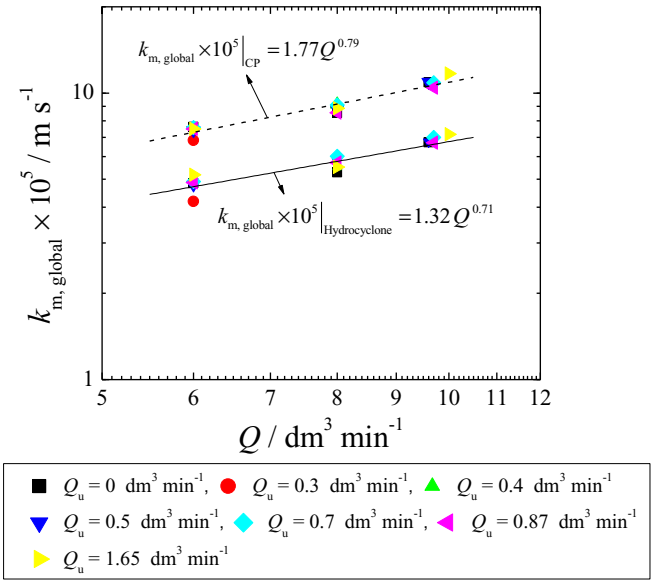

Figure 6. Influence of the inlet volumetric flow rate on the global mass-transfer coefficient. Full line: hydrocyclone. Dashed line: cylindrical part of the hydrocyclone. Ferricyanide reduction as test reaction.

agreement with studies of mass-transfer reported in swirling flow,[20] but the mass-transfer coefficients is lower than those given by Eq. 11. Figs. 3 and 6 allow concluding that the modified hydrocyclone presents excellent mass-transfer conditions being the cylindrical part more effective than the conical one.

Removal of copper.—Fig. 7, part (a) displays typical curves of the concentration change of copper in the reservoir as a function of time for different inlet volumetric flow rates. The classical exponential variation expected for a recirculating electrochemical reactor system is observed,[21] with an important decrease in concentration with time, and after 1 hour of electrolysis the concentration decays one order of magnitude. A similar temporal behavior is detected independent on the volumetric flow rate approaching the concentration 25 ppm at the end of the experiment. This constant value is produced due to the fact that the smallest copper particles are not separated by the hydrocyclone and they are re-oxidized in the reservoir by oxygen, anodically generated, increasing copper concentration. Fig. 7, part (b) shows typical curves of the temporal behavior of current at different inlet volumetric flow rates. At the beginning of the experiment the current increases with time because of copper deposition enlarges the electrode surface area. However, the current diminishes at higher times as a consequence of the depletion of copper in the solution. These opposite behaviors explain the peak in the current as it is shown in this figure. The current density distributions in the hydrocyclone during copper deposition were similar to those obtained in the above mass-transfer studies, corroborating that the cylindrical part represents the most active surface area of the equipment.

Fig. 8, part (a), compares the figures of merit at different cathodic potentials after 60 minutes of electrolysis. As expected, a slight increase in cell potential difference is observed when the cathodic potential becomes more negative. The current efficiency shows a maximum at −1.0 V, and consequently the specific energy consumption a minimum, which can be explained considering the enhancement in mass-transfer by bubble-induced convection due to hydrogen evolution at this potential. However, at more cathodic potentials hydrogen evolution becomes important and the current efficiency decreases. Moreover, at −0.85 V the space time yield is slightly lower than at −0.65 V, but with an increase in the specific energy consumption. Then, in order to obtain a maximum in the space time yield of the equipment with reasonable specific energy consumption a potential

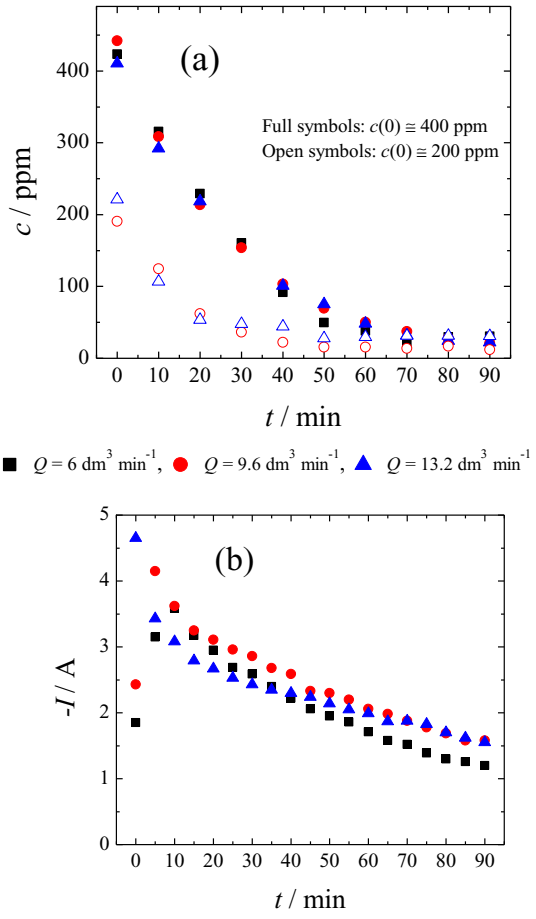

Figure 7. Part (a): Temporal variation of copper concentration in the reservoir at different inlet volumetric flow rates. Part (b): Temporal variation of current at different inlet volumetric flow rates for $c(0)) \cong 400$ ppm. $E_{SCE} = -0.65$ V.

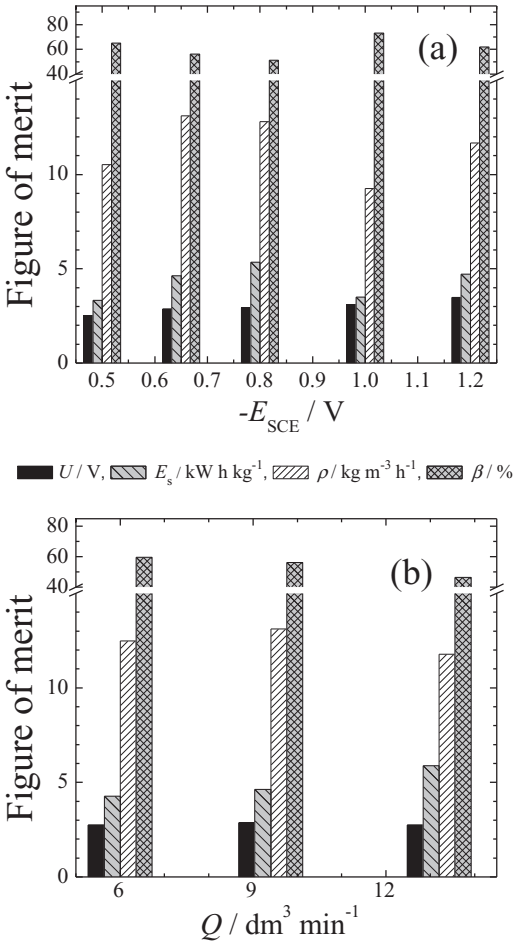

Figure 8. Figures of merit for copper deposition at the modified hydrocyclone. Part (a): as a function of the cathodic potential, $Q = 9.5$ dm^3 min^{-1}. Part (b): as a function of the inlet volumetric flow rate, $E_{SCE} = -0.65$ V. Electrolysis time: 60 min. $c(0) \cong 400$ ppm.

of −0.65 V can be considered as an optimal value. Fig. 8, part (b) reports on the figures of merit as a function of the inlet volumetric flow rates for a cathodic potential of −0.65 V after 60 minutes of electrolysis. A change in volumetric flow rate modifies the limiting current density for copper deposition and it also affects the morphological characteristics of the deposits. Thus, for the accuracy expected in experiments involving metal deposition, a similar behavior is observed changing the volumetric flow rate. Thus, the cell potential difference was 2.78 V with 4.9 kW h kg^{-1} and 12.5 kg m^{-3} h^{-1} for the specific energy consumption and space time yield, respectively, after 60 minutes of electrolysis. The cumulative current efficiency was 54%, due to oxygen reduction takes place as a side cathodic reaction. Under these working conditions the copper concentration in the reservoir was reduced one order of magnitude given 1 h^{-1} for the normalized space velocity of the recirculating system. The above specific energy consumption is in the middle range of the values reported for copper removal from dilute solutions using different electrochemical reactors, according to Dhamo et al.[4]

During an experiment, a fraction of the metal deposited on the cathode was detached from the electrode as a powder, whose largest particles were separated by the hydrocyclone and they were obtained from the underflow. As expected, the amount of powder separated by the hydrocyclone increases with the volumetric flow rate. Taking into account this finding and the results reported on Fig. 8, part (b), it results convenient to operate the hydrocyclone at the maximum inlet flow rate. As a typical example, for $Q = 13.2$ dm^3 min^{-1} after 90 minutes of electrolysis the amount of copper reduced at the cathode was 1.82 g, obtained from the change of concentration in the electrolyte. Moreover, it was observed that the copper was completely detached from the first three segments at the cylindrical part of the reactor and approximately 12% was the fraction of copper obtained as a powder from the spigot.

Characterization of the metal powder

The metal powder obtained from the spigot of the hydrocyclone was profusely washed with distilled water and was dried in a vacuum oven. The surface morphology and the particle size were examined by scanning electron microscopy. Fig. 9 shows that the morphology of the particles in the copper powder is strongly dependent on the working conditions. Thus, at a volumetric flow rate of 9.6 dm^3 min^{-1} the particles exhibit mainly a crystalline morphology with parallelepipedical shape as it is depicted in part (a). A statistical analysis of the particle size, based on a sample of 615 independent measurements, reveals that the particle dimensions are in the range from 0.15 μm to 1.05 μm with a mean value of 0.5 μm and a standard deviation of 0.22 μm. When the volumetric flow rate was increased to 13.2 dm^3 min^{-1} the copper powder obtained from the spigot presented a dendritic structure as it is shown in Fig. 9 part (b). This change of morphology may be attributed that a higher volumetric flow rate can detach by erosion larger structures of the deposited copper, which are more easily separated by the hydrocyclone. The EDAX study of the samples revealed copper as the main element in the powder, 97 wt%, with small amounts of lead and iron due to the dissolution or mechanical degradation of the anode.

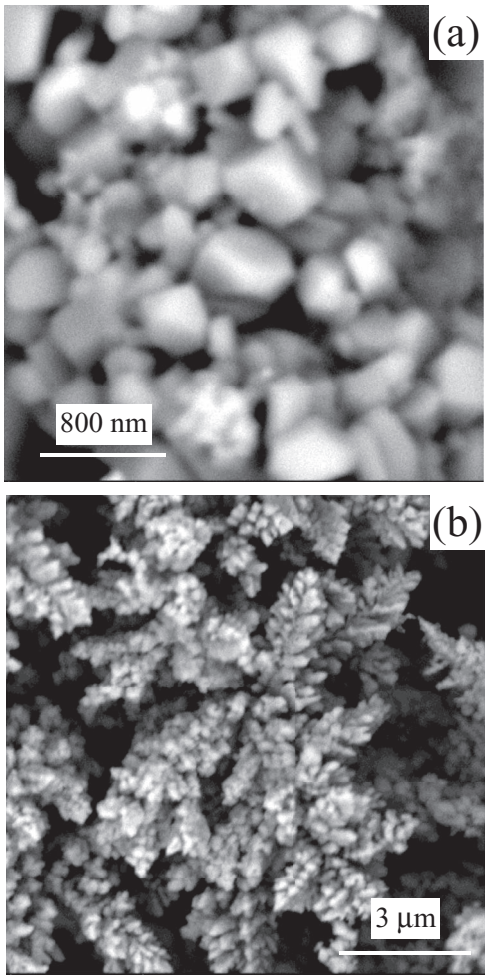

Figure 9. Scanning electron micrographs of copper powders obtained from the spigot of the hydrocyclone. Part (a): $Q = 9.6$ dm^3 min^{-1}, Magnification: ×90000. Part (b): $Q = 13.2$ dm^3 min^{-1}, Magnification: ×25000. $E_{SCE} = -0.65$ V. $c(0) \cong 400$ ppm.

Conclusions

For the experimental conditions of the present study the following conclusions are made:

(i) The local mass-transfer coefficient changes with the axial position from the reactor entrance, showing the cylindrical part of the hydrocyclone the highest values, which abruptly diminish in the conical region.

(ii) The global mass-transfer coefficient in the cylindrical part is higher than that reported for a developing axial flow in an annular duct, revealing an important improvement of the mass-transfer behavior due to the helical flow.

(iii) The global mass-transfer coefficient in the cylindrical part shows a similar dependence with the Reynolds number to that reported in decaying annular swirl flow.

(iv) The modified hydrocyclone was able to diminish the copper concentration from 400 ppm to a minimum of approximately 25 ppm after 90 min of electrolysis. The metal ions were reduced at the cathode and a fraction of the deposit, approximately 12%, was recuperated as a metal powder, separated as a suspension by the hydrocyclone.

(v) The modified hydrocyclone can be recognized as a promising electrochemical reactor for effluent treatment allowing the removal of the contaminant and simultaneously its transformation and recovery as a product of commercial value.

Acknowledgments

This work was supported by the Agencia Nacional de Promoción Científica y Tecnológica (ANPCyT), Consejo Nacional de Investigaciones Científicas y Técnicas (CONICET) and Universidad Nacional del Litoral (UNL) of Argentina.

List of Symbols

A_i	surface area of the i-th segment, m^2
c	concentration, mol/m^3 or ppm
D	diffusion coefficient, m^2/s
d_e	equivalent diameter $= d_o - d_i$, m
d_i	inner diameter, m
d_o	outer diameter, m
E_{SCE}	electrode potential against saturated calomel electrode, V
E_s	specific energy consumption, kW h/kg
F	Faraday constant, 96485 C/mol
I	total current, A
$I_{lim,\,i}$	limiting current at the i-th segment, A
$k_{m,\,y}$	local mass-transfer coefficient, m/s
$k_{m,\,global}$	global mass-transfer coefficient, m/s
L	electrode length, m
M	molar mass of copper, g/mol
Q	inlet volumetric flow rate, dm^3/min
Q_u	underflow stream, dm^3/min
Re	Reynolds number $= u_{av} d_e/\nu$
s_n	normalized space velocity, h^{-1}
Sc	Schmidt number $= \nu/D$
Sh	Sherwood number $= k_m d_e$/D
t	time, min or h
u_{av}	average fluid velocity in the annulus, m/s
U	cell potential difference, V
V	total electrolyte volume, m^3
V_r	reactor volume, m^3
y	axial coordinate, m

Greek

β	cumulative current efficiency, %
ν	kinematic viscosity, m^2/s
ν_e	charge number of the electrode reaction
ρ	space time yield, kg/m^3/h

Subscripts

CP	cylindrical part

References

1. D. Bradley, *The Hydrocyclone*, Pergamon Press, Oxford (1965).
2. C. Aldrich, in *Progress in Filtration and Separation*, S. Tarleton Editor, p. 1, Academic Press, Oxford (2015).
3. N. Dhamo and R. Kammel, *Metall*, **46**, 912 (1992).
4. N. Dhamo, M. Bakalli, and L. Bushi, *J. Environ. Prot. Ecol.*, **2**, 1000 (2001).
5. N. Dhamo, *J. Appl. Electrochem.*, **24**, 745 (1994).
6. N. Dhamo, *Waste Manage. (Oxford)*, **16**, 257 (1996).
7. G. Rajalo, T. Petrovskaya, and V. Ahelik, *Proc. Estonian Acad. Sci. Chem.*, **46**, 122 (1997).
8. K. Sundmacher, *J. Appl. Electrochem.*, **29**, 919 (1999).
9. Y. Kim, H. Cho, H. Lee, C. Lee, J. Lee, K. Rhee, H. Sohn, and T. Kang, *J. Appl. Electrochem.*, **32**, 1235 (2002).
10. S.-K. Kim, C. K. Lee, J.-C. Lee, K.-I. Rhee, H.-J. Sohn, and T. Kang, *Resour. Process.*, **51**, 48 (2004).
11. B.-C. Yu, S.-K. Kim, J.-S. Sohn, B.-S. Kim, K.-I. Rhee, and H.-J. Sohn, *J. Appl. Electrochem.*, **44**, 741 (2014).
12. R. Battino, T. R. Rettich, and T. Tominaga, *J. Phys. Chem. Ref. Data*, **12**, 163 (1983).
13. J. R. Selman and C. W. Tobias, in *Advances in Chemical Engineering*, T. B. Drew, G. R. Cokelet, J. W. Hoopes, and T. Vermeulen, Editors, p. 211, Academic Press, New York (1978).

14. H. J. Wiesner, in *Modern Electroplating*, 3rd. ed., F. A. Lowenheim, Editor, p. 266, John Wiley, New York (1974).
15. J. Mehlig, *Ind. Eng. Chem. Anal. Ed.*, **13**, 533 (1941).
16. J. M. Bisang, *J. Appl. Electrochem.*, **26**, 135 (1996).
17. A. N. Colli and J. M. Bisang, *Electrochim. Acta*, **154**, 468 (2015).
18. S. Yapici, M. A. Patrick, and A. A. Wragg, *J. Appl. Electrochem.*, **24**, 685 (1994).
19. A. A. Mobarak, H. A. Farag, and G. H. Sedahmed, *J. Appl. Electrochem.*, **27**, 201 (1997).
20. S. Yapici, M. A. Patrick, and A. A. Wragg, *J. Appl. Electrochem.*, **25**, 15 (1995).
21. A. N. Colli and J. M. Bisang, *Electrochim. Acta*, **58**, 406 (2011).